Published in final edited form as:

J Magn Reson Imaging. 2018 November ; 48(5): 1351–1357. doi:10.1002/jmri.26030.

SHEAR STRAIN RATE FROM PHASE CONTRAST VELOCITY ENCODED MRI: APPLICATION TO STUDY EFFECTS OF AGING IN THE MEDIAL GASTROCNEMIUS MUSCLE

Usha Sinha, PhD[1], **Vadim Malis, MS**[2,3], **Robert Csapo, PhD**[2,4], **Marco Narici, PhD**[5], and **Shantanu Sinha, PhD**[2]

[1]Physics, San Diego State University, California, USA

[2]Muscle Imaging and Modeling Lab, Dept. of Radiology, UC San Diego, San Diego, California, USA

[3]Physics, UC San Diego, San Diego, California, USA

[4]Institute for Sports Medicine, Alpine Medicine and Health Tourism, University for Health Sciences, Medical Informatics and Technology, Hall, Austria

[5]School of Graduate Entry Medicine and Health University of Nottingham, Derby, UK

Abstract

BACKGROUND—Strain rate (SR) is a measure of the rate of regional deformation that can be computed by analyzing velocity encoded phase-contrast 2D images. Recent studies have explored the changes in normal components of the strain tensor in aging muscle while shear strain may also provide valuable information.

PURPOSE—To compute the shear strain rate from velocity encoded MRI of the lower leg and to study the correlation of strain rate (SR) parameters measured in the medial gastrocnemius (MG) to muscle force in a cohort of young and senior subjects.

STUDY TYPE—Prospective cohort study.

SUBJECTS—Six young (26.1 ± 2.3 yrs) and six senior (76.7 ± 8.3 yrs) healthy females; two other subjects were scanned on three separate occasions for repeatability studies.

FIELD STRENGTH/SEQUENCE—1.5T using a single oblique sagittal slice with velocity encoding in three directions (Velocity encoded phase contrast gradient echo sequence).

ASSESSMENT—Age related and regional differences in the SR eigenvalues (SR_{fiber}, $SR_{in\text{-}plane}$), normal strain rates (SR_{ff}, SR_{cc}) and shear strain rates (SR_{fc}, SR_{fc_max}) were statistically analyzed.

STATISTICAL TESTS—Difference between young and senior cohorts were assessed using two-way analysis of variance (ANOVAs). Coefficient of variation and repeatability coefficient were calculated from repeat studies. Univariate and stepwise multivariable linear regression was performed to identify predictors of force.

Corresponding Author: Shantanu Sinha Ph.D., RIL, Dept. of Radiology, UCSD, 3510 Dunhill Street, San Diego, CA-92121, Ph.No.: 858-534-2004, shsinha@ucsd.edu.

RESULTS—During isometric plantarflexion contraction, strain rates in the principal basis (SR_{fiber}, $SR_{in\text{-}plane}$) and maximum shear strain rate (SR_{fc_max}) was significantly lower in the senior cohort ($p<0.05$). On multiple variable regression, maximum shear strain rate (SR_{fc_max}) and normal strain rate in the fiber cross-section (SR_{cc}) were significantly associated with force ($R=0.681$, $F=14.034$, $p<0.001$).

DATA CONCLUSION—This study establishes that computation of shear strain is feasible and is a significant predictor of force variability with age.

Keywords

Strain rate tensor; Shear strain rate; Aging Muscle; Velocity encoded MRI; lateral transmission of force

Introduction

The strain or strain rate (SR) tensor is a measure of the rate of regional tissue deformation and a 2×2 SR tensor is computed by analyzing a velocity encoded 2D phase contrast MR image and this analysis has been applied to study skeletal muscle deformation (1). In the frame of reference represented by the principal basis, the diagonal terms represent the strain rate in two orthogonal directions (normal strains) while the cross-terms that represent the shear strain rate are zero (2). In order to extract the shear strain rate, the tensor is rotated to the muscle fiber basis defined by the muscle fiber orientation. Other approaches to mapping the muscle fiber direction strain include combined deformation analyses and diffusion tensor imaging based tractography (3,4). In the latter paper, the authors attribute the observed fascicular heterogeneity to epimuscular myofascial force transmission (4). Furthermore, the rotation of the tensor by 45° from the principal basis yields the maximum value of the shear strain rate. This provides a number of parameters including strain rate tensor components in the principal basis, in the muscle fiber basis, and the maximum shear strain. Specifically, the SR tensor provides information on tissue deformation along two orthogonal axes as well as on tissue shear through the off-diagonal terms of the tensor (5). These strain rate components reflect underlying muscle fiber properties like contractility and extracellular matrix material properties like stiffness. As these properties are known to change with conditions such as disuse, age, and disease, strain rate components could potentially enable non-invasive monitoring of muscle tissue contractility and material properties.

The loss of muscle force that occurs with aging is disproportionately greater than the loss of muscle mass (atrophy) and is still not completely understood (6). Neural and contractile contributions to age related loss of muscle force have been explored extensively (7). One potential determinant of age related loss of muscle force that has not been investigated in depth is the remodeling of the extracellular matrix (ECM) and its functional consequences (8). Several studies have emphasized the importance of force transmission pathways: longitudinal transmission of force via the myotendinous junction and lateral transmission of force mediated by the extracellular matrix via myofascical pathways (8, 9). Impairment in lateral transmission pathways with age have been demonstrated in aging rodents and has been linked to the remodeling of the ECM (9). The shearing of the ECM has been postulated to be the underlying mechanism of lateral transmission of force; thus, measurement of the

shear strain could potentially be a surrogate assessment of lateral transmission of force. It should be emphasized though that the role of the ECM may not be limited to modulating the lateral transmission of force but it may be involved in a more general force transmission mechanism termed 'myofascial force transmission' (4).

This paper extends an earlier study that explored the changes in muscle strain rate with age where the analysis was limited to normal strain rates in the principal basis (5). The earlier study identified the strain rate components in the principal basis that significantly differed between young and old subjects. Thus, this paper focused on: (i) establishing the repeatability limits of strain rate components in human subjects, (ii) evaluating strain rate tensor components in the different bases to monitor age related differences in muscle deformation, and (iii) identifying the relationship between the SR parameters and muscle force in a cohort of young and senior subjects.

Methods

Subjects

The study was approved by the Medical Research Ethics Board of University of California at San Diego (UCSD) and conformed to the standards in the Declaration of Helsinki on the use of human subjects in research. All subjects were included in this study after obtaining informed consent. Six young (26.1 ± 2.3 yrs, height: 158.6 ± 5.6 cm, mass: 50.8 ± 3.7 kg) and six senior (76.7 ± 8.3 yrs, height: 153.0 ± 2.0 cm, mass: 57.4 ± 4.3 kg) healthy, moderately active, female subjects were included in this study after informed consent (5). Two subjects (one young: 25 years, one old: 65 years) were scanned on three separate days to determine the coefficient of variation (CV) and the repeatability coefficients (RC) of the SR components.

MR imaging

MR imaging was performed on a 1.5 Tesla Signa HDx MR scanner (GE Medical Systems, Milwaukee, WI) as described in (5, 10). Images were acquired during submaximal, isometric, plantarflexion contraction at 35% of the individual maximum voluntary contraction (MVC); this level was chosen so that all subjects could comply with the imaging protocol (72 contractions/ cycle). Imaging was performed with the subject lying supine, feet first, with the non-dominant leg to be imaged placed in a cast. An optical fiber pressure transducer was glued to the sole of the cast that was firmly anchored to the radiofrequency coil by means of Velcro straps (Velcro USA Inc, Manchester, NH). Pressure exerted against the cast during isometric contraction was detected by the transducer, converted to a voltage by a spectrometer (Fiberscan, Luna Innovations, Roanoke, VA), and used to trigger the MR image acquisition. Subjects were provided real-time visual feedback of the force generated superposed on the target force curve to facilitate consistent contractions (Supplemental Video 1). MR imaging included high-resolution water saturated oblique sagittal fast spin echo (FSE) images of the medial gastrocnemius (MG) where muscle tissue (water) signal is suppressed while the fascicles (fat) appear hyperintense. The slice (oblique sagittal) that best depicted the fascicles was selected for the Velocity-Encoded Phase Contrast (VE-PC) scan (5). The VE-PC acquired single oblique sagittal slice (TE: 7.7 ms, TR: 16.4 ms, NEX: 2,

FA: 20°, slice thickness: 5 mm; FOV: 30 cm×22.5 cm, 4 views/segment, 1 slice, 22 phases (temporal resolution of 131 ms and an isometric plantarflexion cycle of ~3 secs), 10 $cm.s^{-1}$ three directional velocity encoding, 72 repetitions).

Force measurements

MVC was determined for each subject as the best of three trials recorded prior to imaging (5, 10). During the execution of the ~70 contraction-relaxation cycles, torques were recorded at a sampling frequency of 200 Hz and averaged to produce curves of mean torque. To estimate muscular forces, the measured torque was divided by the Achilles tendon moment arm length, which was measured on an oblique sagittal-plane FSE MR images of the ankle (one slice passing through the center of the ankle joint) and defined as the perpendicular distance between the axis of the tendon and the joint's center of rotation, assumed to coincide with the midpoint of a circle fitted around the talus.

Computation of the Strain rate tensor

Strain rate (SR) Calculation in the Principal Basis

The (2×2) SR tensor was calculated from the spatial gradient of the velocity images (velocity validated using calibrated flow phantoms, (11)) and then diagonalized to obtain the eigenvalues (SR_{fiber}, $SR_{in\text{-}plane}$) and eigenvectors. SR_{fiber} denotes deformation in a direction closer to the muscle fiber axis (than the orthogonal SR component) and is negative during muscle fiber shortening and positive during relaxation. $SR_{in\text{-}plane}$ denotes deformation in the muscle fiber cross-section and is positive during muscle fiber shortening and negative during relaxation. In this paper, only a 2×2 SR tensor is computed since a single velocity encoded slice (selected such that the MG muscle fibers lie in the plane of the image) was acquired precluding the computation of the z-derivative of velocity required for the complete 3×3 tensor.

Muscle Fiber Tracking

MG muscle fibers (end points on the aponeuroses) are located on the fast spin-echo images at the distal, middle and proximal regions, transferred to the first frame of the dynamic images and the end points are tracked through the isometric, plantarflexion cycle (5).

Strain rate in the fiber basis

Strain rate in the fiber basis was computed by rotating the SR tensor in the principal axes frame to the fiber basis using the following rotational transformation (Figure 1).

$$SR_{fb} = R \cdot SR_{pb} \cdot R^{T} \quad [1]$$

$$R = \begin{pmatrix} \cos\theta & -\sin\theta \\ \sin\theta & \cos\theta \end{pmatrix} \quad [2]$$

where SR_{fb} is the strain rate tensor in the fiber frame defined by the fiber axis, *f*, and the fiber in-plane cross-sectional axis, *c*; R is the 2D rotation matrix defined by the SR-fiber angle θ, and SR_{pb} is the strain rate tensor in the principal basis frame. SR_{fb} has diagonal elements SR_{ff} and SR_{cc} (normal strain along the fiber and in the cross-section respectively) and non-diagonal terms SR_{fc} (shear strain) while SR_{pb} has the diagonal terms SR_{fiber} and $SR_{in\text{-}plane}$ (negative and positive principal strain rates respectively) (Fig. 1).

Strain rate tensor in the maximum shear strain rate basis

The maximum shear strain, SR_{fc_max} was estimated by rotating SR_{pb} by 45° (from tensor algebra, the maximum in the off-diagonal terms occurs 45° from the principal axes (12)). SR_{fiber}, $SR_{in\text{-}plane}$, SR_{ff}, and SR_{cc} are called normal strains (defined as perpendicular to the face of an element and represented by the diagonal terms of the SR tensor) while SR_{fc} and SR_{fc_max} are shear strains (defined as parallel to face of an element and represented by off-diagonal terms in the SR tensor); the former is the shear strain in the muscle fiber basis and the latter is the maximum shear strain (Figure 1). Supplemental Figure 1 shows the SR analysis pipeline and the anticipated variability in the computed SR components as a function of the variability in the velocity images.

ROI measurements

Regional analysis of normal and shear strains in the two bases was performed on ROIs selected manually on the magnitude images at the proximal, middle, and distal regions (corresponding to distances at 75%, 50% and 25% of the total MG muscle length from the distal end) of the medial gastrocnemius. Since the ROIs shifted with muscle motion, pixel tracking was performed to ensure that the same anatomical region was being sampled (Supplemental Video 2). The SR indices were computed at two force levels: one at the peak force level for each subject and the other at a force level of the subject with the lowest maximum MVC exerted by any subject. 'Peak values' of the SR components were identified at the temporal frame of the negative eigenvalue peak (SR_{fiber}) in the compression phase. To extract values at the same force level for a subject, the temporal frame corresponding to the lowest MVC (of all subjects) was located in the force-time curves and SR values were extracted from the closest frame of the dynamic MRI.

Statistical analyses

The coefficient of variation (CV) was calculated as the ratio of the within subject standard deviation, S_w, to the mean value expressed as a percentage (estimated from the three repeat measures). The repeatability coefficient, RC, which represents the threshold value below which the absolute differences between 2 measurements on the same subject is expected to lie for 95% of the measurement pairs was calculated as (0.0277*mean*CV) (13). For all tests, the level of significance was set at 0.05. Univariate and stepwise multivariable linear regression was performed to identify predictors (MG strain rate parameters estimated at the peak of the SR) of force in a cohort of young and senior subjects. The predictors tested were the strain parameters alone and did not include morphological parameters since the latter are already established as predictors; the focus here was to test if SR components were predictors and of these, to identify the most significant SR predictor(s). For the multivariable

analysis, only independent variables were retained. The statistical analyses were carried out using SPSS for Mac OSX (SPSS 23.0, SPSS Inc., Chicago, IL).

Results

Muscle force was lower by 43% in the senior cohort: young (387 ± 43 N) and senior (220 ± 43 N), $p<0.05$. This was accompanied by an 18% lower volume of the triceps surae muscles of the senior cohort, implying that the entire force loss could not be accounted by a decrease in muscle volume. Figures 2 and 3 show the colormaps of the normal strain rates in the principal basis (SR_{fiber}, $SR_{in\text{-}plane}$) and the maximum shear strain rate (SR_{fc_max}) for one young and one senior subject at the same force level (Figure 2) and at the peak force (Figure 3). Supplemental Figure 1 shows the errors propagated at each step of the SR analysis starting from the uncertainty in the calculation of the velocity maps. Supplemental Figure 2 shows the temporal variation of the strain rate components as a function of the isometric, plantarflexion contraction.

Table 1 lists the average values of the strain rate components for the young and senior cohorts at the same force level and at the peak of the force. The mean value of all the regions (distal, middle and proximal) is reported since there was no regional variation in any of the SR parameters or any 'age × region' interactions. CV and RC for SR_{fiber} and SR_{fc_max} were ~6% and ~17% respectively; the RC value indicates that differences in these indices greater than 17% between cohorts can be identified. However, the variability of $SR_{in\text{-}plane}$ was much higher; this may potentially reflect the larger velocity uncertainties due to in-plane motion artifacts.

Statistical analysis for the SR indices obtained at the same force and at peak force level showed significant age-related differences in: SR_{fiber}, $SR_{in\text{-}plane}$ and in SR_{fc_max}, and in addition, in SR_{ff} for the peak force analysis alone. Table 2 summarizes regression models for SR indices obtained at peak force level (2a) and at same force level (2b). SR_{ff} (negatively) and SR_{fc_max} (positively) were significantly correlated with force output, with SR_{fc_max} having the strongest correlation. Scatter plots of the univariate regression models for same force level and at peak force level are shown in Supplemental Figure 3 and in Supplemental Figure 4 respectively. Stepwise multivariable regression produced a model with two predictors SR_{fc_max}, SR_{cc} and with R=0.681 (moderately good level of prediction).

Discussion

Examining the factors contributing to the variability in the measurements, we conclude that the primary sources arise from: inconsistency of the isometric, plantarflexion contractions, the intrinsic uncertainties in the SR measurement methodology, as well as from subject specific differences. Karakuzu et. al. recently noted that inter-individual differences in the muscle-tendon complex anatomy may, in part, be responsible for inter-subject strain variability (4). The first contribution to variability was minimized by the visual feedback. Propagation of error analysis similar to that in (14) shows that the uncertainty in the SR is approximately eight times the uncertainty in the velocity. This high variability is reflected in

the ROI measurements though 3D anisotropic diffusion filtering of the velocity maps was performed to reduce the uncertainty in the velocity maps.

The results of the strain rate analysis in the principal basis and in the fiber basis show that normal strains along the fiber (SR_{fiber} and SR_{ff}) and in the fiber cross-section ($SR_{in\text{-}plane}$) are significantly lower in the aging cohort. Azizi et al showed by combining a mathematical model with experimental manipulation that the structural changes in the ECM (e.g., increase in collagen and in stiffness) compromise the muscle's ability to expand radially, which in turn restricts muscle shortening (15). Thus, the observed changes in both normal strains (along the fiber as well as in the fiber cross-section) can be attributed, at least in part, to the structural changes in the ECM. Significant differences in the maximum shear strain rate were found between young and senior cohorts. The SR tensor including shear strain is measured at the voxel level precluding a direct assignment of the shear strain to the endomysium (very short T2 and much smaller widths than MR voxel resolution). However, computational models have identified that endomysium (or ECM) shears and it is a reasonable extrapolation to associate the measured MR shear strain to the shear in the ECM. This latter shear has been proposed to be the mechanism by which force is transmitted laterally (16, 17). While a direct non-invasive measurement of lateral transmission of force (LTF) is not possible, the current analysis of shear strain rate may potentially be a surrogate measure of LTF. The ability to compute the shear strain rate, as reported in this paper, may provide a tool to explore, non-invasively and in-vivo, modifications to lateral transmission pathways. It is important to point out that a simplified model of a single muscle fiber and surrounding endomysium is considered here. In reality, when considering groups of active muscle, the situation is more complex and the shearing of the endomysium may potentially be attributed to the presence of complex intramuscular myofascial loads. Karakuzu et al argue that epimuscular myofascial loads and intramuscular ones originating from the ECM and muscle fibers impact local deformations and are the underlying source of strain variability within a muscle (4). Their hypothesis of force transmission through the myofascial network is consistent with the interpretation in this paper of the observed shear strain as potentially arising from the shearing of the endomysium.

It should be noted that the mechanical role of the ECM is not limited ‘lateral transmission of force’. Some of the findings observed in the current paper such as increased strain rates in the anterior compartment muscles of the triceps surae may be explained by a more general force transmission mechanism: ‘myofascial force transmission’. The latter force transmission pathway considers the skeletal muscle within a myofascial continuity, where ECM mechanically interacts with muscle fibers along their full lengths which are in turn, subject to further mechanical alterations through the surrounding muscles via epimuscular pathways (18). Wilke et al have recently shown that these mechanical interactions in turn have significant effects on the mechanical properties of the connective tissue (19). It is highly likely that with age, the mechanical properties of the connective tissue (in the endomysium, perimysium and epimysium) are altered resulting in differences in strain rate components.

The current study shows that the basis frame in which the strain rate component is a maximum (principal basis for normal strains or shear strain maximum) is the most sensitive

to detect age related changes (e.g., SR_{fiber}, $SR_{in\text{-}plane}$, SR_{fc_max} show significant differences). Comparison at the same force level across all subjects makes the evaluation at a fairly low force level for most of the subjects and may not potentially be the optimum force level to detect changes. In contrast, evaluation at the peak of the force ensures the same effort level (%MVC) across subjects and further, is not limited by the force exerted by the weakest subject. Though significant differences in SR_{fiber}, $SR_{in\text{-}plane}$ and maximum shear strain rate were seen in evaluations by both methods, it may be physiologically meaningful to make the comparisons at the peak force level. In univariate analysis, several SR parameters were significantly correlated to force confirming that both normal and shear strain rates significantly predict muscle force output. It is also noteworthy that, in multivariable regression, the two significant predictors of force in a cohort of young and senior subjects are strain rate indices SR_{cc} and SR_{fc_max}; both are known from other studies to be related to the status of the extracellular matrix (15–17).

It should be emphasized that the strain rate is in reality a 3×3 tensor, whereas only the 2×2 SR tensor is computed here. The inability to compute the full 3×3 tensor arises from the fact that a single slice is acquired, which though encoded for velocity in three orthogonal directions does not allow the computations of the velocity gradient in the slice direction (thus precluding a 3×3 tensor analysis). In the current protocol, multiple slices can be acquired in multiple scans but this will extend scan times such that senior subjects cannot tolerate. 3D SR mapping awaits the development of new faster imaging sequences enabling 3D volume acquisitions with 3 directional velocity encoding in scan times of 3–4 minutes. It is acknowledged that the identification of the fascicles as entirely in-plane (of the oblique sagittal slice in the current study) is not completely accurate as fascicles are known to be non-planar (20). In this context, it should be noted that the oblique sagittal slice for VE-PC was identified following a specific protocol that resulted in the best depiction of the fascicles in the fast spin echo images. This protocol included (i) selecting the axial slice with the largest cross-section of the MG from a stack of axial slices of the calf muscle, (ii) positioning the oblique slice such that it bisected the distance between the femur and tibia and was perpendicular to it, and importantly, (iii) aligning the oblique slice with or parallel to the most prominent dark line line depicting a fascicle in this axial slice. In the stack of such sagittal oblique “scout” slices, one of the slices generally had several prominent dark fascicular lines, which was subsequently used for the VE-PC acquisition. Sometimes a second stack of scout slices had to acquired, to get the best depiction of the fascicles in the oblique sagittal planes (these “scout” scans were quite rapid). The accuracy of the orientation of the VE-PC slice was ensured by checking for the most number and highest contrast of the dark fascicular lines in the oblique sagittal FSE images. The reproducibility of this slice orientation and position was confirmed after subject repositioning as part of the reproducibility studies. Ensuring the reproducibility of the orientation of the 2D VE-PC slice is important as the 2D tensor is sensitive to the orientation of the dynamic slice. While adherence to the above protocol ensured reproducible slice identification, accuracy of the slice orientation was also confirmed by examining the through-plane velocity values (sequence encodes velocity of the 2D oblique slice in all three directions). For the studies reported here, the through-plane velocity was negligible compared to the in-plane velocities. This is consistent with results from full 3D strain tensor studies where the strain in the

through-plane direction is almost zero (21). If the orientation of the VE-PC slice was not accurate, through-plane velocity values would not be small compared to the in-plane velocity values. While in the current paper, the slice orientation was reproducible and minimized through-plane motion, it is acknowledged that 3D strain rate tensor computed from 3D volume acquisition combined with three direction velocity encoding will provide a more accurate representation of muscle deformation.

The paper focuses on establishing the feasibility of shear strain mapping with application to aging muscle. The variability of the computed indices is high, but despite the variability, the computation of the 2×2 SR tensor as opposed to the full 3×3 SR tensor, and the small number of subjects, significance was reached in detecting age related differences. This is a first report of the significant differences in shear strain between young and old cohorts and its significance in accounting for age related force variability in the cohorts. In order to disambiguate potential sex based differences in age related muscle deformations, this preliminary study is limited to female subjects. Future work will extend this to larger cohorts with equal representations from both sexes and will be designed to address potential covariates (muscle mass, neural components, fatty infiltration, connective tissue, intrinsic contractility of the fiber). The most important finding of our study is the association of muscle force output to shear strain rate (in addition to normal strain rate) confirming that lower values of the shear strain rate may also contribute to age related loss of muscle force.

Supplementary Material

Refer to Web version on PubMed Central for supplementary material.

Acknowledgments

Grant Support: National Institute of Arthritis and Musculoskeletal and Skin Diseases Grant 5RO1-AR-053343-08

References

1. Drace JE, Pelc NJ. Skeletal muscle contraction: analysis with use of velocity distributions from phase-contrast MR imaging. Radiology. 1994; 193:423–429. [PubMed: 7972757]
2. Taber LA. Nonlinear Theory of Elasticity: Applications in Biomechanics. World Scientific Publishing Co. Pte. Ltd.; 2004. 107
3. Pamuk U, Karakuzu A, Ozturk C, Acar B, Yucesoy CA. Combined magnetic resonance and diffusion tensor imaging analyses provide a powerful tool for in vivo assessment of deformation along human muscle fibers. J Mech Behav Biomed Mater. 2016; 63:207–219. [PubMed: 27429070]
4. Karakuzu A, Pamuk U, Ozturk C, Acar B, Yucesoy CA. Magnetic resonance and diffusion tensor imaging analyses indicate heterogeneous strains along human medial gastrocnemius fascicles caused by submaximal plantar-flexion activity. J Biomech. 2017; 57:69–78. [PubMed: 28433388]
5. Sinha U, Malis V, Csapo R, Moghadasi A, Kinugasa R, Sinha S. Age-Related Differences in Strain Rate Tensor of the Medial Gastrocnemius Muscle During Passive Plantarflexion and Active Isometric Contraction Using Velocity Encoded MR Imaging: Potential Index of Lateral Force Transmission. Magn Reson Med. 2015; 73:1852–1863. [PubMed: 25046255]
6. Degens H, Erskine RM, Morse CI. Disproportionate changes in skeletal muscle strength and size with resistance training and ageing. J Musculoskelet Neuronal Interact. 2009; 9:123–129. [PubMed: 19724146]

7. Lieber RL, Ward SR. Cellular mechanisms of tissue fibrosis. 4. Structural and functional consequences of skeletal muscle fibrosis. Am J Physiol Cell Physiol. 2013; 305:C241–C252. [PubMed: 23761627]
8. Hughes DC, Wallace MA, Baar K. Effects of aging, exercise, and disease on force transfer in skeletal muscle. Am J Physiol-Endoc M. 2015; 309:E1–E10.
9. Ramaswamy KS, Palmer ML, van der Meulen JH, Renoux A, Kostrominova TY, Michele DE, Faulkner JA. Lateral transmission of force is impaired in skeletal muscles of dystrophic mice and very old rats. J Physiol-London. 2011; 589:1195–1208. [PubMed: 21224224]
10. Sinha S, Shin DD, Hodgson JA, Kinugasa R, Edgerton VR. Computer-controlled, MR-compatible foot-pedal device to study dynamics of the muscle tendon complex under isometric, concentric, and eccentric contractions. J Magn Reson Imaging. 2012; 36:498–504. [PubMed: 22392816]
11. Sinha S, Hodgson JA, Finni T, Lai AM, Grinstead J, Edgerton VR. Muscle kinematics during isometric contraction: development of phase contrast and spin tag techniques to study healthy and atrophied muscles. J Magn Reson Imaging. 2004; 20:1008–1019. [PubMed: 15558560]
12. Wolf L, Kazimi MS, Todreas NE. Introduction to structural mechanics. Massachusetts Institute of Technology: MIT OpenCourseWare. 2012. https://ocw.mit.edu
13. Bland JM, Altman DG. Statistical methods for assessing agreement between two methods of clinical measurement. Lancet. 1986; 8476:307–310.
14. Jensen ER, Morrow DA, Felmlee JP, Odegard GM, Kaufman KR. Error analysis of cine phase contrast MRI velocity measurements used for strain calculation. J Biomech. 2015; 48:95–103. [PubMed: 25433567]
15. Azizi E, Deslauriers AR, Holt NC, Eaton CE. Resistance to radial expansion limits muscle strain and work. Biomech Model Mechanobiol. 2017; 16:1633–1643. [PubMed: 28432448]
16. Sharafi B, Blemker SS. A mathematical model of force transmission from intrafascicularly terminating muscle fibers. J Biomech. 2011; 44:2031–2039. [PubMed: 21676398]
17. Gao Y, Waas AM, Faulkner JA, Kostrominova TY, Wineman AS. Micromechanical modeling of the epimysium of the skeletal muscles. J Biomech. 2008; 41:1–10. [PubMed: 17904147]
18. Yucesoy CA. Epimuscular myofascial force transmission implies novel principles for muscular mechanics. Exerc Sport Sci Rev. 2010; 38:128–134. [PubMed: 20577061]
19. Wilke J, Schleip R, Yucesoy CA, Banzer W. Not merely a protective packing organ? A review of fascia and its force transmission capacity. J Appl Physiol (1985). 2018; 124:234–244. [PubMed: 29122963]
20. Rana M, Hamarneh G, Wakeling JM. 3D fascicle orientations in triceps surae. J Appl Physiol (1985). 2013; 115:116–125. [PubMed: 23640593]
21. Englund EK, Elder CP, Xu Q, Ding Z, Damon BM. Combined diffusion and strain tensor MRI reveals a heterogeneous, planar pattern of strain development during isometric muscle contraction. Am. J. Physiol. Regul. Integr. Comp. Physiol. 2011; 300:R1079–R1090. [PubMed: 21270344]

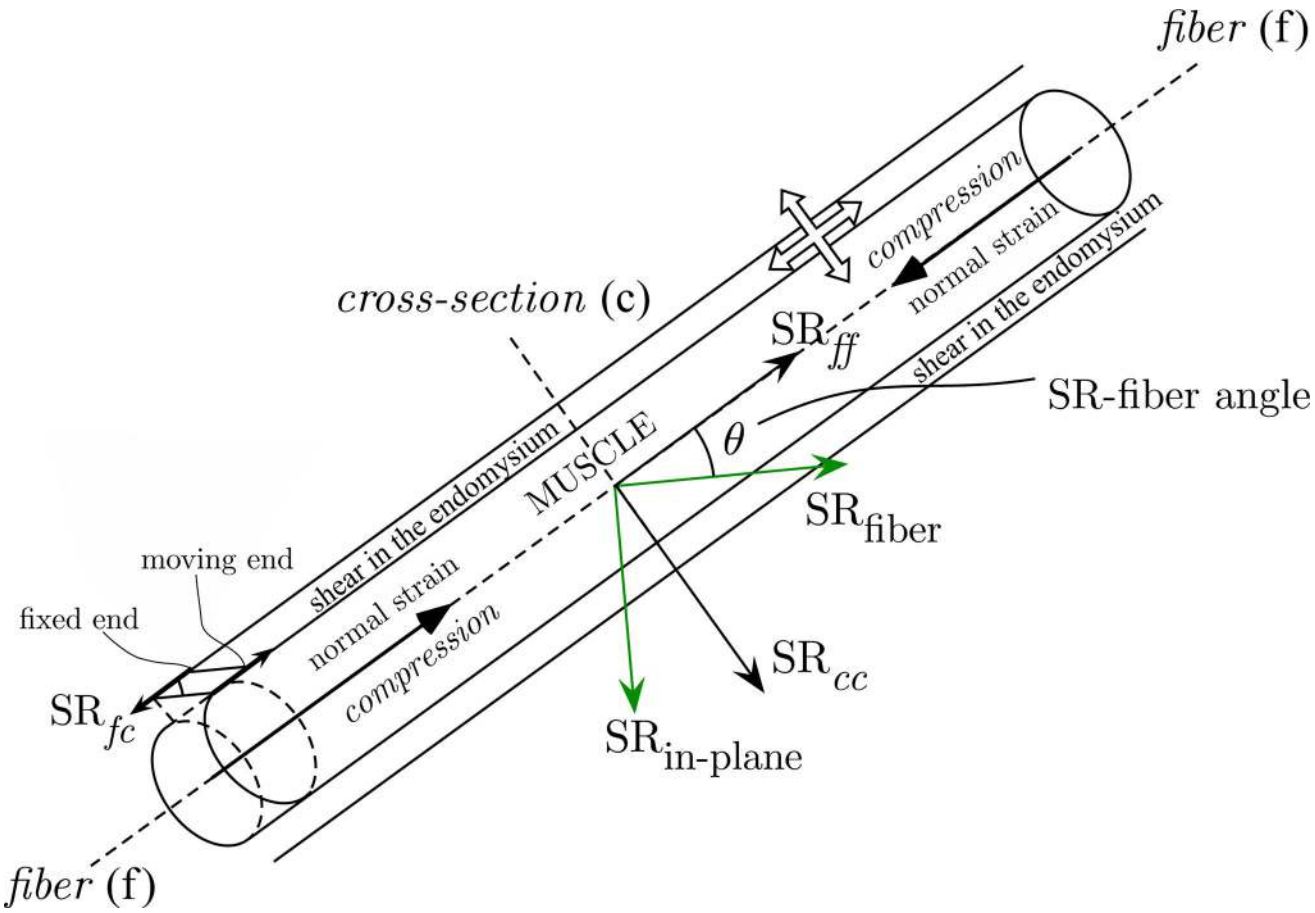

Figure 1.

Schematic of a muscle fiber and endomysium with the principal basis and fiber basis defined with respect to the muscle fiber. The muscle fiber is shown contracting while the endomysium experiences a shear strain (end attached to the muscle contracts with the muscle fiber while the other end stays fixed resulting in a shear strain; ends labeled in the schematic). The direction of the strain rate components in the two basis sets (SR_{fiber} and $SR_{in\text{-}plane}$ in the principal basis and SR_{ff} and SR_{cc} in the muscle fiber basis) as well as the angle between these two basis sets, SR-fiber angle are shown in the schematic. The thick (unfilled) arrows show the lateral transmission of force pathways: from the cross-bridges of the myofilaments through the protein network (costameres) on the sarcolemma to the extracellular matrix. Arrows indicate normal and shear strains.

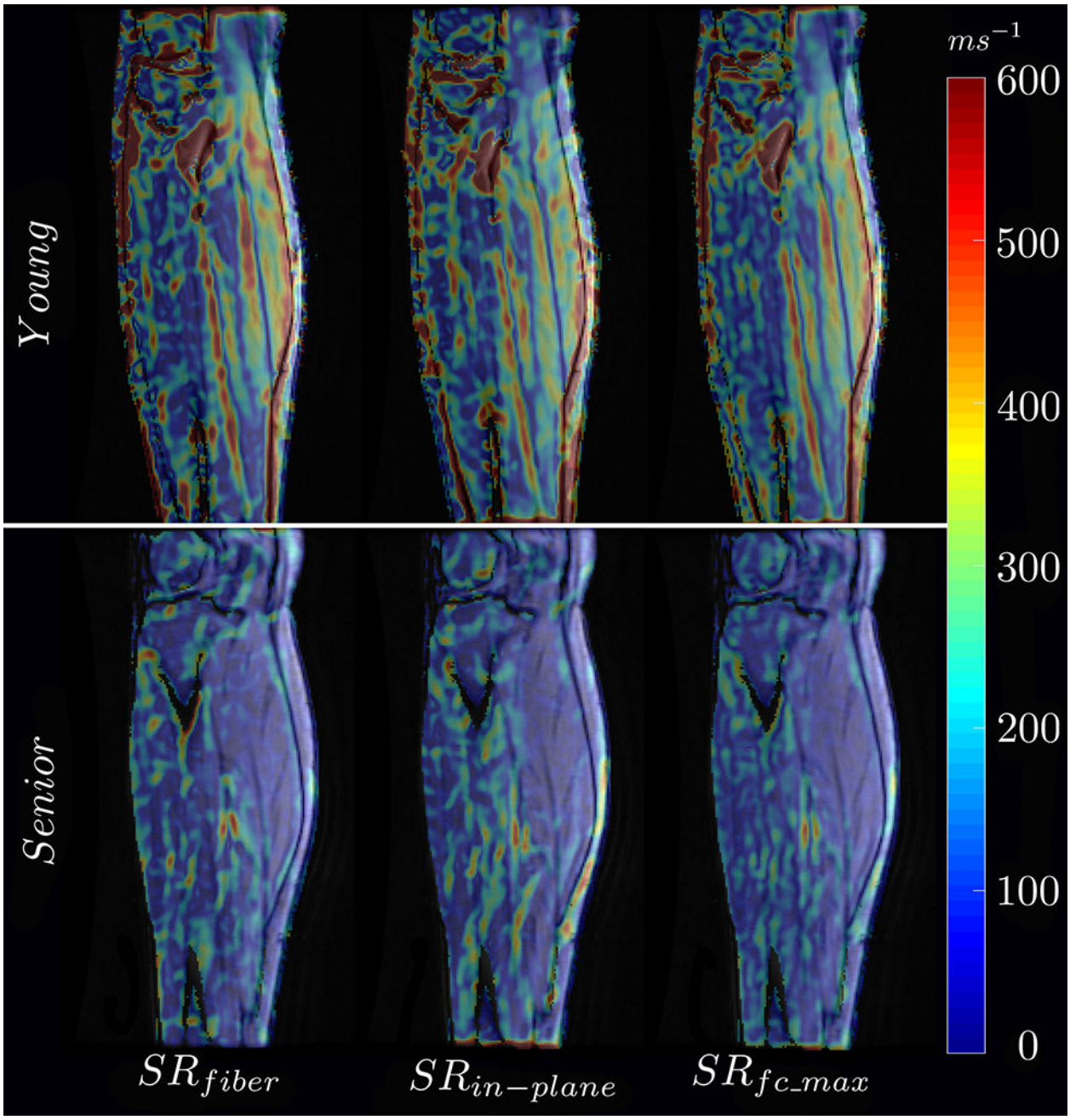

Figure 2.

Strain rate maps of the normal strain rates (SR_{fiber}, $SR_{in\text{-}plane}$) and shear strain rates (SR_{fc_max}) in a young and senior subject at the same force level. The color maps are color-coded according to the legend provided with the figure. Colormaps are overlaid on the magnitude image at the corresponding frame; overlay allows better identification of the underlying muscle, fascicles and aponeuroses. The maps show lower values in both the normal strain rates in seniors.

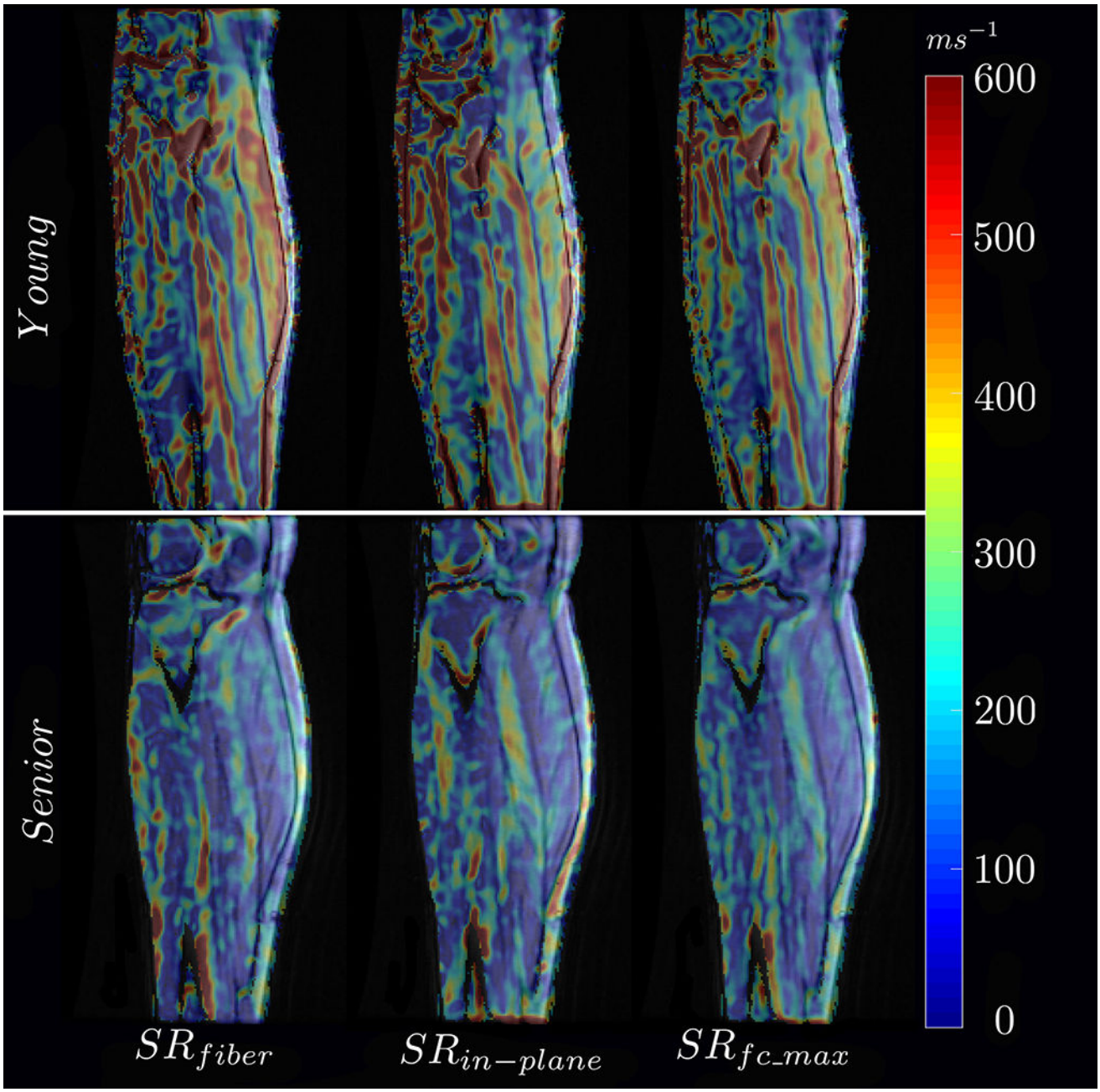

Figure 3.

Strain rate maps of the normal strain rates (SR_{fiber}, $SR_{in\text{-}plane}$) and shear strain rates (SR_{fc_max}) in a young and senior subject at the peak force level. The color maps are shown at the peak of SR_{fiber} in the compression phase of the isometric cycle. The color maps are color-coded according to the legend provided with the figure. Colormaps are overlaid on the magnitude image at corresponding frame; overlay allows better identification of the underlying muscle, fascicles and aponeuroses. The maps show lower values in both normal and shear strain rates in seniors.

Table 1

Strain Rate (SR) indices (units of ms^{-1}) averaged for three regions of interest in the principle, fiber, and maximum shear strain rate bases at same force level and at peak force.

Principle axis basis		**SR_{fiber}** †	**$SR_{in\text{-}plane}$** †	**SR_{fc_max}** †
Senior	same force level	−245 ± 192	186 ± 120	224 ± 133
	peak	−280 ± 196	177 ± 102	235 ± 107
	CV, RC	3.9, 34.8	41.9, 222.8	9.3, 78.0
Young	same force level	−391 ± 151	280 ± 119	335 ± 107
	peak	−424 ± 140	298 ± 125	351 ± 108
	CV, RC	9.6, 135.5	23.5, 173.9	6.2, 58.5
Fiber basis		SR_{ff}	SR_{cc}	SR_{fc}
Senior	same force level	−170 ± 118	121.47 ± 134	111 ± 135
	peak	−181 ± 102 †	91 ± 173	125 ± 145
Young	same force level	−259 ± 146	152 ± 146	182 ± 153
	peak	−288 ± 143 †	146 ± 168	192 ± 156

† – significant difference between age groups ($p<0.05$)

Table 2

a: Univariable and multivariable linear regression analysis of parameters obtained at same force level with a significant association with Maximum Volunteer Contraction. Model R=0.640, F=11.448, p<0.001

	Univariable		Multivariable	
	Beta	**P value**	**Beta**	**P value**
SR_{fiber}	−0.421	0.011		
$SR_{in\text{-}plane}$	0.470	0.001		
SR_{ff}	−0.561	<0.001		
SR_{cc}	0.410	0.013	0.369	0.012
SR_{fc}	−0.339	0.043		
SR_{fc_max}	−0.528	0.001	−0.606	<0.001

b: Univariable and multivariable linear regression analysis of parameters obtained at force peak with a significant association with Maximum Volunteer Contraction. Model R=0.681, F=14.034, p<0.001

	Univariable		Multivariable	
	Beta	**P value**	**Beta**	**P value**
SR_{fiber}	−0.353	0.035		
$SR_{in\text{-}plane}$	0.558	<0.001		
SR_{ff}	−0.554	<0.001		
SR_{cc}	0.465	0.004	0.198	0.009
SR_{fc}	−0.262	0.122		
SR_{fc_max}	−0.583	<0.001	−0.393	0.001